RESEARCH PAPER

Influence of Calcination Temperature on Structural, Morphological and Magnetic Properties of M-Type Strontium Hexaferrite Powder Prepared by Sol-Gel Auto Combustion Route

Mahmood M. Kareem

Department of Physics, College of Education, University of Garmian, Kurdistan region, Iraq

ARTICLE INFO

ABSTRACT

Strontium hexaferrite ($SrFe_{12}O_{19}$) nanopowders have been synthesized using sol-gel auto combustion route. Ferrite precursors were obtained from aqueous mixtures of strontium nitrate and ferric nitrate nonahydrate. Citric acid ($C_6H_8O_7$), was added to the mixed solution as fuel. The effect of calcination temperature on the structural, morphological, magnetic properties and phase formation of synthesized $SrFe_{12}O_{19}$ nanopowder was investigated and discussed in details. The material properties were studied employing X-ray diffraction (XRD), Raman spectroscopy, SEM, and a vibrating-sample magnetometer (VSM). The calcined products and the formation of crystalline phase were analyzed via XRD technique which revealed the SrM single phase formation at calcined temperature $1100^{o}C$ with a crystallite size of 76.107 nm. The Rietveld refinement technique as applied in the Fullprof program was utilized for determining the resulting crystalline phase's amounts, lattice parameters, Bragg R-factor and refined structure value χ2. Raman analysis verified the development of the whole crystallographic hexaferrite locations and the whole peaks in the sample related to Raman vibration modes as well as M-type structures. Additionally, the resulted outcomes verified that the prepared material was $SrFe_{12}O_{19}$ and its density (ρ_x) reduced as its calcination temperature increased up to $1100^{\circ}C$. The sample material's magnetic analysis at the room temperature elucidated a higher coercivity value of (4610 Oe), a saturation magnetization of (66.285 emu/g), and a remnant of 38.90 emu/g.

INTRODUCTION

Nanoscience field comprises innovating as well as making novel nanostructures, but the hard task is to generate a connection between their characteristics to possess multifunctional instruments. And, this lead to introduce a bigger incorporated interdisciplinary science recognized as nanotechnology, which keeps on evolving lastingly [1]. Hexaferrite is still the highly pertinent material for the applied uses and most of stiff ferrite manufacture. They're very remarkable materials for innumerable uses. And, of specific attention is the strontium hexaferrite, which has appealed the attention of numerous investigators due to their fresh electromagnetic characteristics, and their usage in a broad range of uses. And, that's due to its description via high Curie temperature, high saturation magnetization, high

* Corresponding Author Email: mahmood.mohammed@garmian.edu.krd

corrosion resistance and chemical stability [2, 3]. Also, it has been known that it can be utilized as lasting magnets, telecommunication, registering media, and parts in microwave, higher-frequency, and magneto-optical instruments [4-7]. Owing to the qualities that listed before as well as its less cost, strontium hexaferrite is regarded to be a preferred nominee for lasting magnets utilized for the industrial uses that being ecologically friendly, like the rotors of generator employed in the wind energy or electric vehicles [1]. The M-type hexagonal ferrites represent a class of hard magnetic and promising materials, they contribute certainly in distinctive hi-tech and industrialized areas owing to their chemical vitality, inexpensive with easy manufacturing methods, and a high uniaxial magneto-crystalline anisotropy [8]. M-type hexagonal ferrite strontium hexaferrite (SrM) belongs to magnetic oxide known as the "magnetoplumbite" phase of ferrites. The SrM possesses a hexagonal structure with a distance set of P63/mmc [9, 10]. It also possesses the benefit of an elevated Curie temperature of (733 K) and remains the high broadly utilized magnets owing to their less price of manufacture **[11].** The M-type hexaferrite's hard magnetic characteristic is ascribed to the uniaxial magneto-crystalline anisotropy of the Fe3+ ions dispersed throughout (5) symmetry locations: One tetrahedral ($\downarrow$4f1), three octahedral ($\downarrow$4f2, $\uparrow$12k and $\uparrow$2a), and one trigonal bipyramidal ($\uparrow$2b) [12]. In preceding documents, it was noted that there's certain unwanted middle non-ferromagnetic phases, which result in deprived magnetic characteristics and uneven form for the particles of derived SrFe12O19 [13]. In the present research, a single-phase SrFe$_{12}$O$_{19}$ nanopowder with a comparatively uniform size has been prepared successfully via the sol-gel auto combustion technique. For the synthesis of SrFe12O19 nanopowders, the calcination procedure was performed as a result of the single phase nanoferrite SrM produced and studied extensively. As a consequence, the grain size, shape and particle size were well controlled, and different techniques, like XRD, Rietveld method, FE-SEM, Raman spectroscopy, and vibrating sample magnetometer (VSM) were applied for the present study.

MATERIALS AND METHODS

SrFe$_{12}$O$_{19}$ hexaferrite was synthesized using citrate sol-gel auto combustion method. A stoichiometric amount of strontium nitrate, Sr $(NO_3)_2$ (>99%), and ferric nitrate nonahydrate Fe $(NO_3)_3 \cdot 9H_2O$ (>99%), were dissolved into a least quantity of deionized water at a continuous stirring. The citric acid ($C_6H_8O_7$) purchased from Thomas Baker was supplemented to the blended solution as a fuel. pH of the last solution was modified to (7) employing ammonia solution and heated to (90°C) to let the whole water evaporate and leave a viscous dense gel. And, the final viscous gel was heated to (275°C), so that the auto-combustion takes place and makes a fluffy powder. Eventually, the resulted powder was calcined at (1000°C) and (1100°C) for (4 hr) for forming the SrFe$_{12}$O$_{19}$ hexaferrite phase. In the present work, the crystalline phase identification was achieved utilizing the XRD measurement that has been performed in Day Petronic Company-Iran with a diffractometer (XRD model: Analytical Philips- XPERT-PRO) provided with CuKα1 (λ =1.54178 Å) employing a (40 kV) generator voltage and a (40 mA) current, and the scans were run through a range (5.0-79.97°) of 2ϑ, utilizing a step size of [2ϑ, 0.026°]. Raman spectroscopy (Micro-Raman spectroscopy-785 nm laser) was employed for investigating the vibrational spectra of the whole samples, while the surface morphology was studied utilizing FE-SEM (FE-SEM; Model Mira3-XMU, TESCAN, made in Japan). The magnetic measurements were conducted at the room temperature employing Vibrating Sample Magnetometer (VSM) (LBKFB model Meghnatis Daghigh Kavir Company).

RESULTS AND DISCUSSION
Structural studies

Fig. 1 shows the typical XRD spectra of the pure strontium hexaferrite SrFe12O19 powder synthesized using sol-gel auto combustion method. The samples were prepared as-burnt (275), calcined at 1000°C and 1100°C which reveals that the most intense diffraction peaks were at 2θ= 30.34, 31.39, 32.33, 34.19, 35.42, 37.14, 40.40, 55.20, 56.84, 63.15 and 72.02 belong the plains (110), (008), (017), (114), (021), (023), (025), (127), (0211), (220) and (228), respectively. The indicated XRD patterns reveal a single-phase M-type Sr hexaferrite which being in good agreement with the standard data (ICDD 01-079-1411) which has a hexagonal crystal system with space group p 63/mmc (number194). The results confirm the formation of crystalline structure.

And, this permits for the impact assessment of the calcined processing upon the SrM materials' structural characteristics, which exhibits that the calcination can be utilized for improving the crystallinity degree. The diffracted peaks are chiefly indexed to the M-type Sr hexaferrite phase, and all samples were highly oriented along the (017) and (114) reflection planes. Moreover, a slight extra Fe$_2$O$_3$ secondary phase is exist at a position of 2θ=33.170° along the direction (104) plane, according to the reference code (ICDD 98-001-2729), and Fig. 1 depicts this phase as indicated by (red stars) at (as burnt) temperature and 1000°C. The patterns of X-ray diffraction obviously reveal that the Fe$_2$O$_3$ peak intensity

disappeared at the calcination temperature of 1100°C. And, this can be clarified via the grains growth as well as the whole crystallization of the M-type Sr hexaferrite. The disappearance of the second impurity phase at 1100°C shows that the creation of M-type Sr hexaferrite is encouraged via elevating the sample synthesis temperature. Thus, the value of temperature (1100°C) is selected as the optimum conditions. It's obvious that the well-defined, sharp and extreme peaks specify the virtuous crystalline materials.

Crystallite size (*D*), unit cell volume (V$_{cell}$), and X-ray density (ρx), of the whole powder samples are assessed from the subsequent formulas [14, 15]:
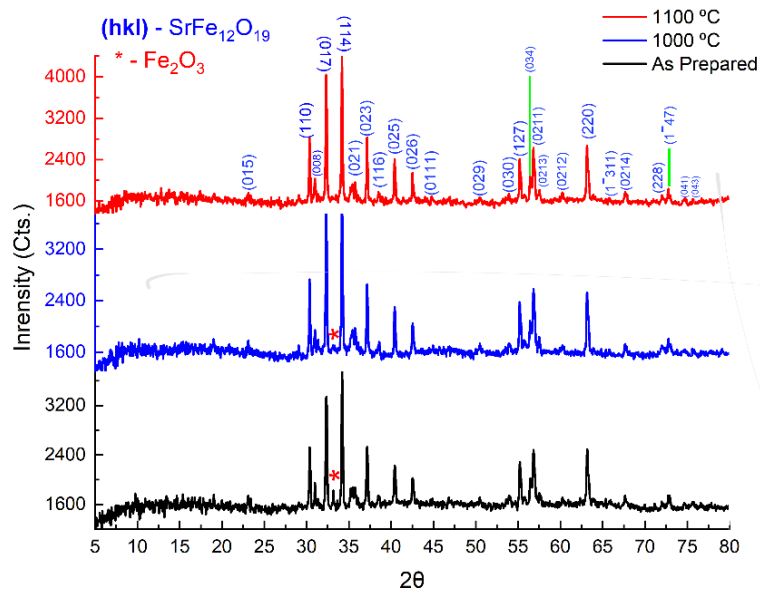

Fig. 1. Patterns of the X-ray diffraction of SrFe$_{12}$O$_{19}$ hexaferrite SrM at :(as burnt, 1000°C and at 1100°C).

Table 1. Structural parameters for SrFe$_{12}$O$_{19}$ hexaferrite (as burnt, 1000°C, and 1100°C).

Tempe. °C	C/a	FWHM	D(nm)	V$_{Cell}$ Å³ (degree)	ρx (gm/Cm³)	$\delta = \frac{1}{D^2}$ 1/cm
As burnt (275)	3.9212	0.143	64.055	691.45	5.087	2.48E+10
1000	3.9209	0.126	43.198	691.21	5.130	5.68E+10
1100	3.9208	0.118	76.107	691.18	5.182	1.755E+10

$$D = \frac{0.9\lambda}{\beta \cos\theta} \tag{1}$$

$$V_{cell} = 0.8666a^2c \tag{2}$$

$$\rho_x = \frac{nM}{N_A \, V_{cell}} \tag{3}$$

Where:

D: Crystallite size

λ: X-ray wavelength of Cu kα radiation

β: Full Width at Half Maximum (FWHM)

ϑ: The angle of diffraction angle (deg.)

M: Molecular mass

N_A: Number of Avogadro

Also, ($\delta = 1/D^2$) is dislocation density, which represents a linear crystallographic defects within the crystal structure [16]. The stated variables change in terms of calcined temperature is shown in Table 1. The broadening of the peaks indicated that all the particles were in nanometer range. The perceived crystallite size (D) verified that the fabricated SrFe$_{12}$O$_{19}$ compound possesses nano-crystalline nature. While the obtained parameters like the lattice parameters a and c, the volume of unit cell and the density of x-ray (ρ_x) for the all samples were in a good agreement and has very small shifts compared with the results founds from the standard data (ICDD 01-079-1411). It is
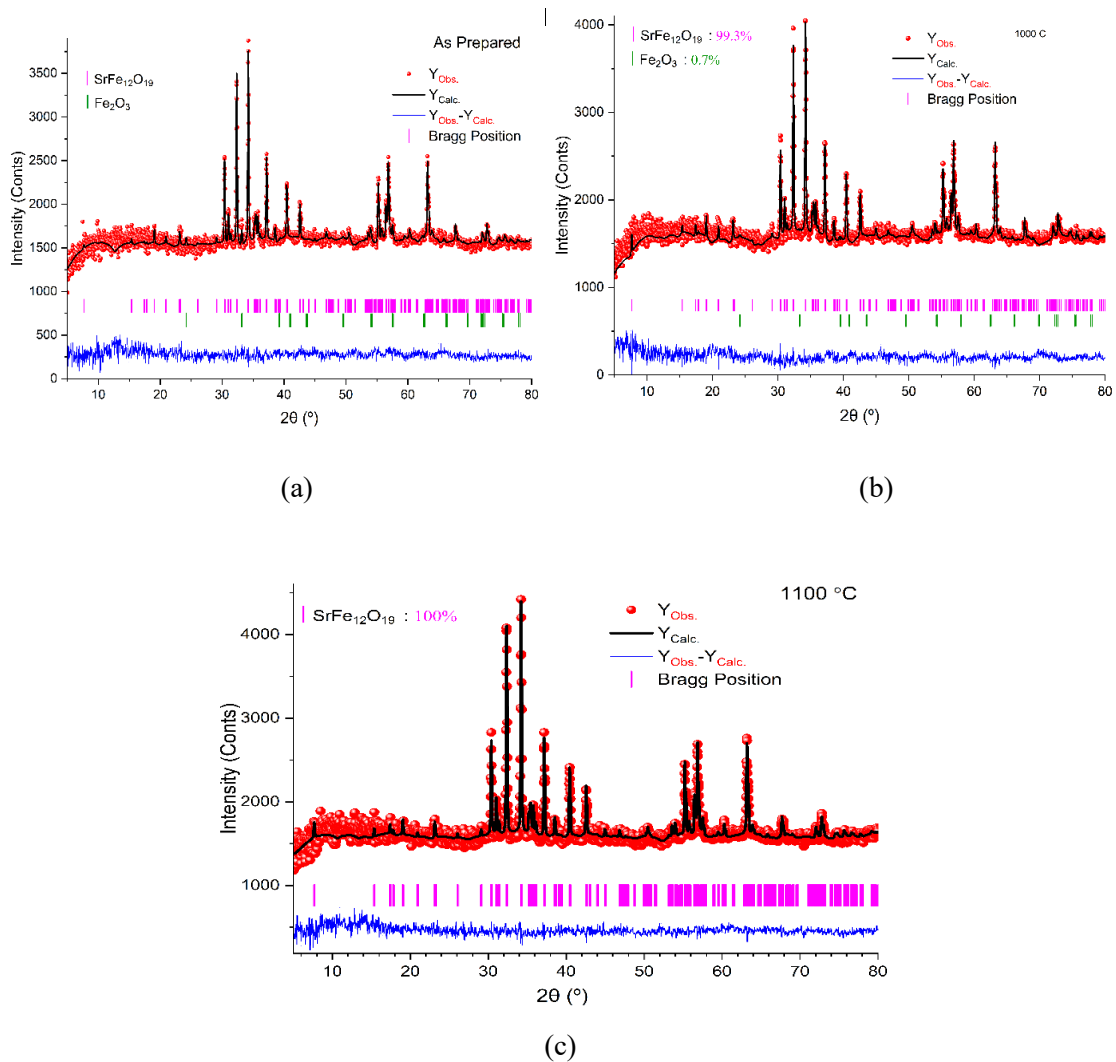

(a)

(b)

(c)

Fig. 2. Patterns of Rietveld refinement of the whole samples calcined at temperatures: (a) as burnt, (b) 1000°C, and (c) 1100°C.

also worth mentioning that the density being a significant parameter which is needed to verify the fabrication of fresh materials. The density values computed for the fabricated powder as well as the densities for the samples calcined at (2) various temperatures, which go on increasing with the increasing calcined temperature, are given in Table 1. Also, the raising density may be the outcome of reduced porosity, since the calcined temperature increases the voids no. or the free volume decrease resulting a higher density[17].

XRD patterns of all samples, which are displayed in Fig. 2(a, b, c), were analyzed using Rietveld refinement with the aid of the Full-Prof Suite software. Through the refinement, the wavelength correction, lattice parameters, zero correction, atomic position, and scale factor were refined at the same time. And, the peaks' shape was characterized via pseudo-Voigt function, as well as the background was stated via a linear interpolation between the chosen background points of a group.

The fitting was arbitrated via the fit goodness,

lengthways with the χ2 factor which is the refined structure factor that derived via the Rietveld method (less than 10 is sensible), as comprised in Table 2. And, it can be seen from the peaks in Fig. 2, and that the profiles for the noted and computed ones are flawlessly corresponded with each other as well as the whole investigational peaks. The small values of χ2 exhibit that the optimized value of extraction is too near to the sample's actual value, and the fabricated sample is too virtuous. Also, Table 2 includes the values for the fit qualities of the fit which is the Bragg R-factor. A virtuous covenant between the noted and calculated reflection, as revealed via determining a minor value for one of the R_{Bragg} indexes, gives a valued sign that the model is making a virtuous job of remaking the crystallographic remarks [17]. And, the R-factors values are < 10% of the existed pattern as well as a refined pattern verified the refinement goodness, as documented via different investigators [18-21]. Additionally, Table 2 includes the weights percentage (w%) of the secondary phase Fe$_2$O$_3$ which it has very small amounts

Table 2. Rietveld results.

Temperature (°C)	χ2	Bragg R- Factor	SrFe$_{12}$O$_{19}$, wt.%	Fe$_2$O$_3$, wt.%
275	1.6	27.9	98.7	1.3
1000	2.3	34.3	99.3	0.7
1100	1.6	26.7	100	0

Table 3. Rietveld refinement results.

Temperature (°C)	SrFe$_{12}$O$_{19}$, %		Fe$_2$O$_3$ %	
	Cell parameter a (Å)	Cell parameter c (Å)	Cell parameter a (Å)	Cell parameter α (degree)
275	5.88174	23.0637	5.43048	55.0702
1000	5.88124	23.0598	5.40929	55.5668
1100	5.88121	23.0592	0	0

and decreases gradually with increasing calcined temperature, it is clear that this secondary phase disappears totally at 1100°C, and this is led to the formation of the pure single phase of Sr Hexaferrite. In summary, at calcined temperature higher than 1000°C, a comparatively neat M-type hexagonal ferrite phase can be determined [22].

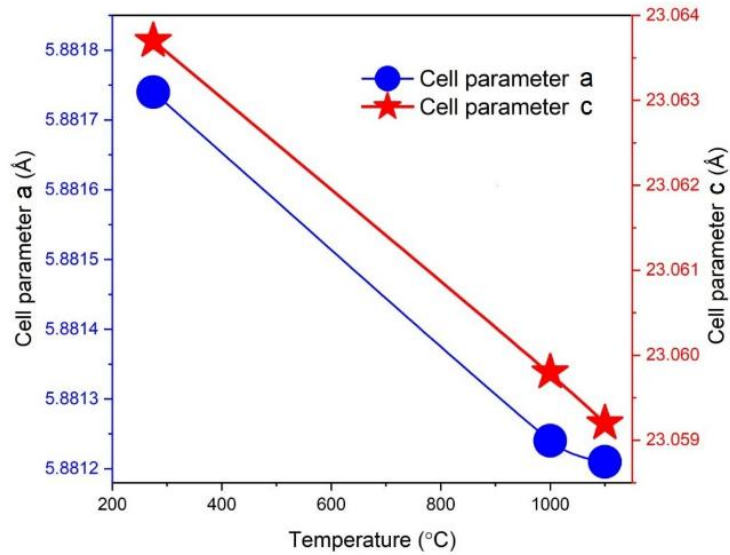The refined lattice parameter values of the

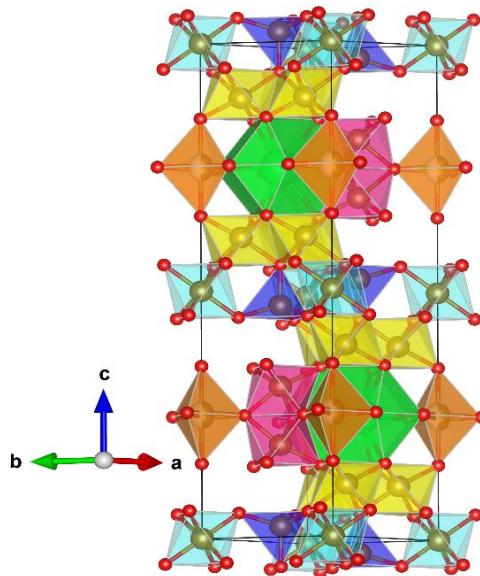Fig. 3. Variation of lattice cell parameters a and c with calcined temperature.

Fig. 4. The unit cell structure of SrM- the different colors represent (Fe) sites: (a) Turquoise-octahedral (Fe1), (b) Orange-trigonal (Fe2), (c) Blue- tetrahedral (Fe3), (d) Green-hexagonal (Sr), (e) Pink-Fe4, and (f) Yellow-Fe5.

intrinsic M-type Sr hexaferrite and Hematite Fe2O3 are listed in the Table 3. And, the values of lattice constant (a) and (c) are obtained in the (a = 5.88121–5.88174 Å) range as well as (c = 23.0592–23.0637 Å) range, correspondingly. Such values are similar to the standard values of (a = 5.88640 A), (c = 23.050 A), in accordance with the ICSD code (98.004-3590) and this in virtuous covenant with the obtained values via [1, 23, 24].

The cells volume was obtained in the (V = 691.45–691.18 Å^3) range which is clear that their values decrease with increasing calcined temperature for all samples. The values of cell parameters (a and c) are decreased with increasing calcined temperature as shown by the Fig. 3, also the c/a values decreased as the calcined temperature is increased and their values vary from (3.9212 Å) to (3.9208 Å). Such values are similar to the standard value (3.9800) of the M-type hexagonal structure [25].

Further studies have been carried out through the present studies, since the process of fitting has been conducted without refining the atomic locations of the SrM structure, due to the difficulties to find an accurate interatomic distances of the samples [26]. The structure profile of hexaferrite SrFe$_{12}$O$_{19}$ is shown in Fig. 4, the atomic sites, bond types, and bond lengths (Å) were obtained and analyzed by applying VESTA software-program for crystal structure model, as well as the results are listed in Table 4 and are in good agreement with literature study [1, 10, 27, 28].

Table 4. Atomic type, sites, bond type and bond lengths (Å) for SrFe$_{12}$O$_{19}$ hexaferrite nanopowder.

Atom	site	Bond type	Bond lengths(Å)
Sr	2d	Sr1-O3	2.946
Fe1	2a	Sr1-O5	2.812
Fe2	2b	Fe1-O1	1.801
Fe3	4f1	Fe1-O4	1.998
Fe4	4f2	Fe2-O1	2.132
Fe5	12k	Fe2-O3	1.867
O1	4e	Fe3-O4	1.890
O2	4f	Fe4-O3	2.050
O3	6h	Fe4-O5	1.975
O4	12k	Fe5-O1	1.975
O5	12k	Fe5-O4	2.113

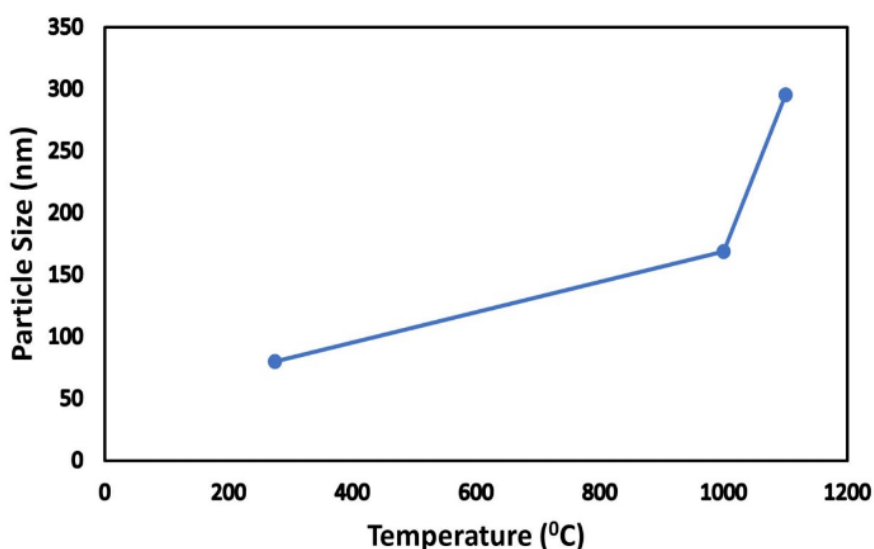

Fig. 5. Calcination temperature vs. particle size.

FE-SEM and EDS analysis

The surface morphology and elemental composition of the SrFe$_{12}$O$_{19}$ hexaferrite nanostructure were revealed using electron microscopy in conjunction with energy dispersive X-ray spectroscopy. The samples were prepared at 275°C (as burnt) and calcined at 1000°C and 1100°C, as depicted in the Fig. 5. It's clear from this figure that the particles possess a distinct form. And, it can be observed that the whole samples have no exact hexagonal shapes, but the structures with increasing calcined temperature

aggregate to show a certain geometrical shapes, as plate-like as well as polyhedral shapes. The uneven dispersion and inhomogeneous way in the size particles may be owing to the fabrication technique influence. And, the fast growth in the crystalline hexaferrite development employing sol-gel auto burning method has resulted in the change of the distribution of the size of particles that are connected with the time length. The adequate elevated temperature being needed for completing the preparation [29]. The existence of certain agglomerated particles collected in
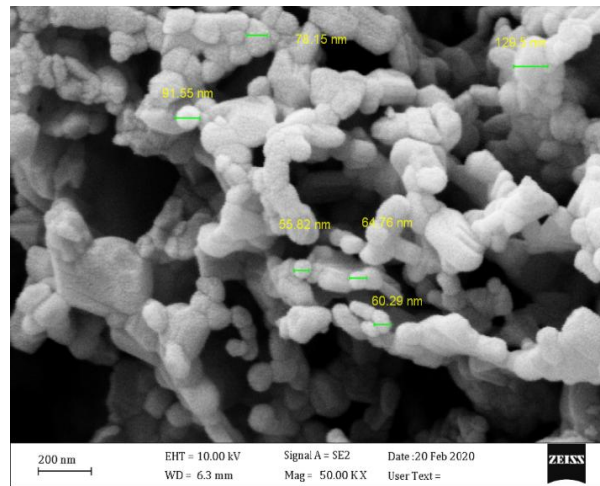
(a)
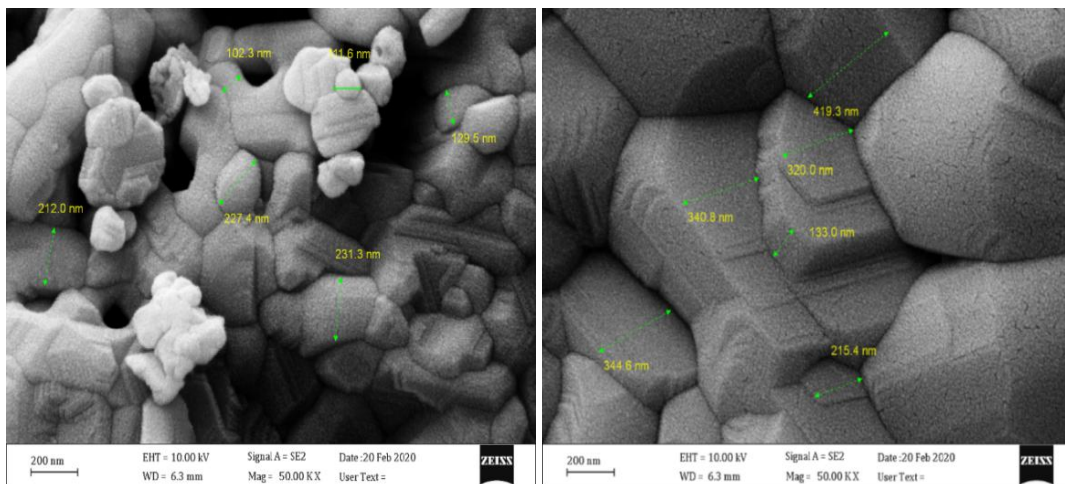
(b)

(c)

Fig. 6. Images of the FE-SEM of the SrFe$_{12}$O$_{19}$ hexaferrite prepared at: (a) as burnt 275°C (b) 1000°C and (c) 1100°C.

the images of FE-SEM is ascribed to the magnetic interactions presence among the particles [30]. And, the substantial reductions in the samples' voids are attributed to the big masses collecting with increasing calcined temperature up to 1100°C, it is obvious that the voids of sample are disappeared at this temperature, and the crystal size was enlarged very dramatically demonstrating
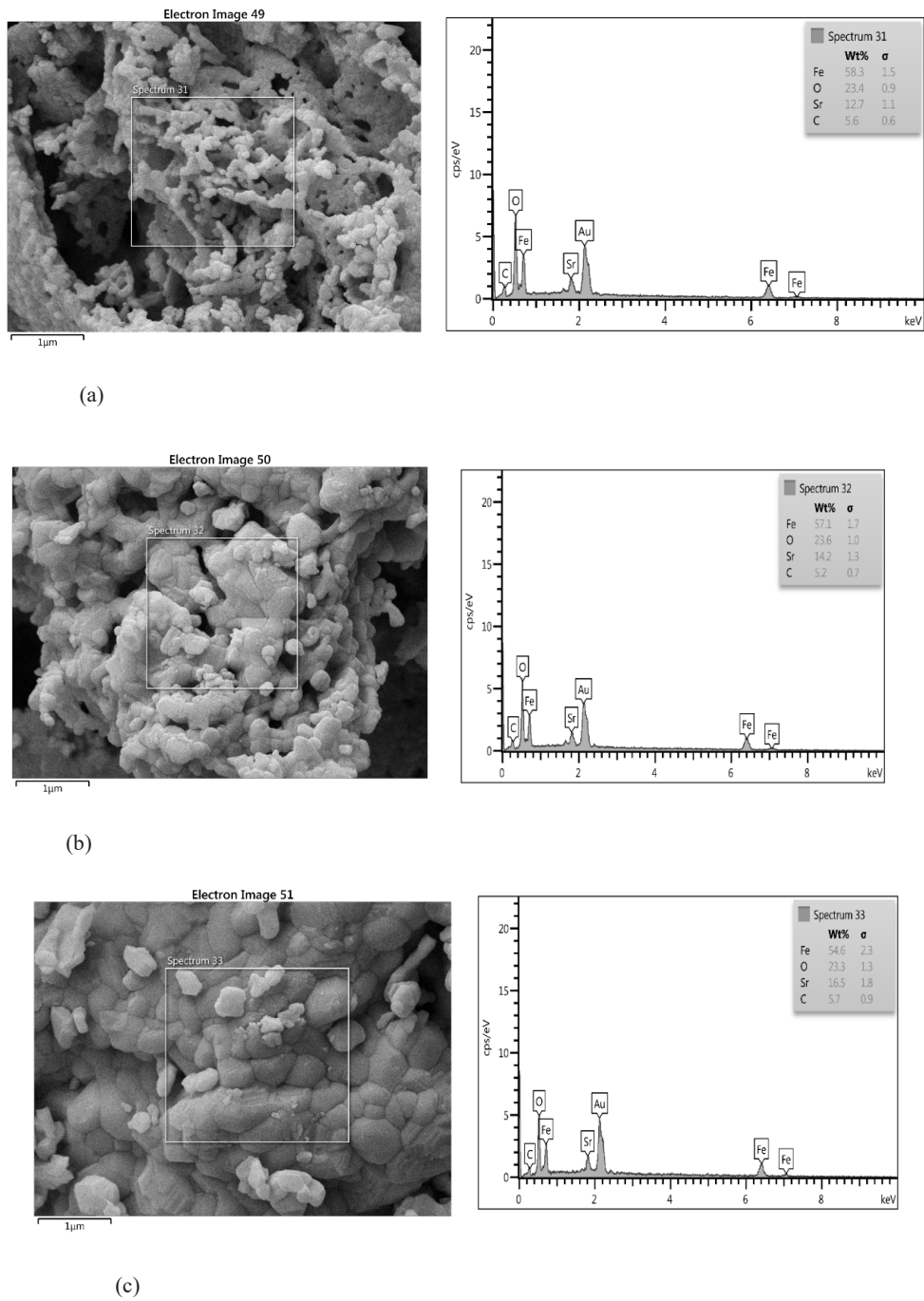

(a)

(b)

(c)

Fig. 7. Corresponding EDS spectrum of the Strontium Ferrite SrFe$_{12}$O$_{19}$ for: as-burnt at (a) 275°C and calcined at (b) 1000°C and (c) 1100°C.

that the size of particle and the morphology were subtle to the calcined temperature, which is coincide with increasing the particle size from 79.84 nm to 295.5 nm with raising the calcined temperature up to 1100°C, as shown in Fig. 6.

Typically, the corresponding EDS spectrum is presented in Fig. 7, which expressly confirms that the material composition contain Strontium (Sr),
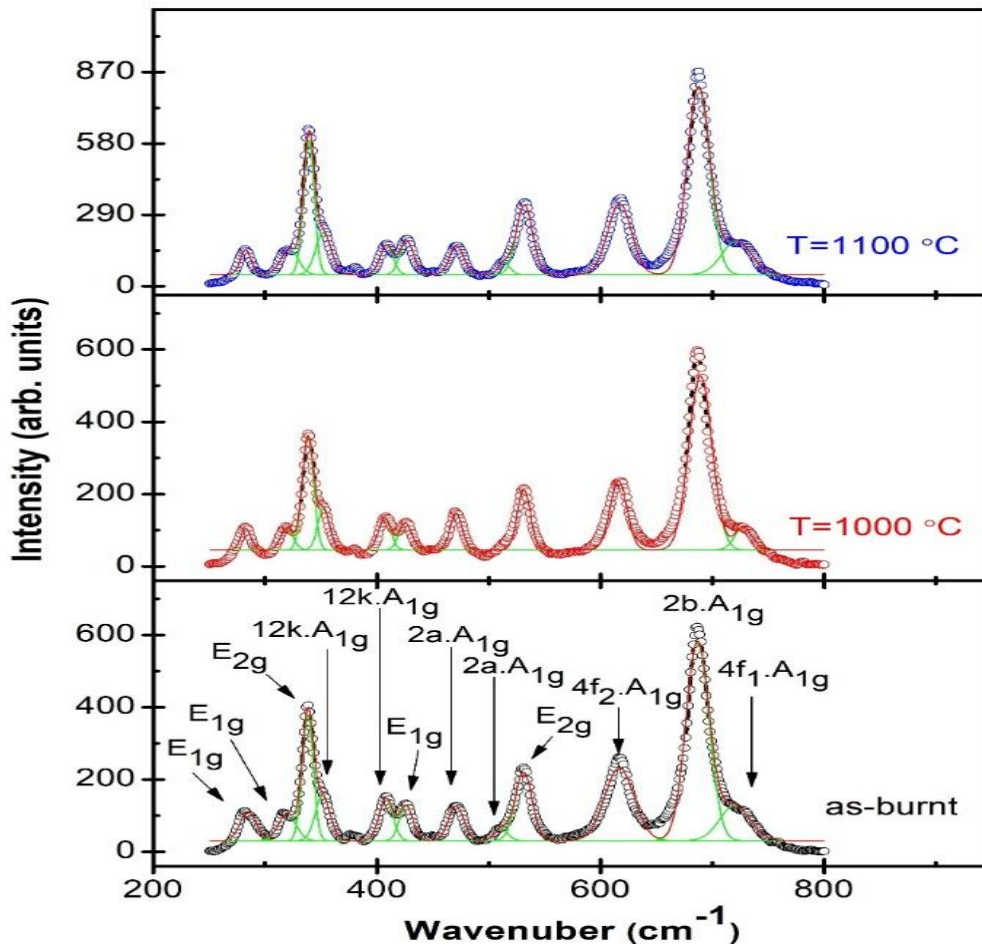
Fig. 8. Raman spectra of SrFe$_{12}$O$_{19}$ nanopowder for: a) as-burnt 275°C and calcined,at (b) 1000°C and (c) 1100.

Table 5. Elemental compositions for SrFe$_{12}$O$_{19}$ at three different calcined temperature.

Elements	Experimental wt.% at temperatures			Theoretical wt.%
	275°C	1000°C	1100°C	
Fe	58.3	54.6	57.1	63.13
O	23.4	23.3	23.6	28.63
Sr	12.7	16.5	14.2	8.25
C	5.6	5.2	5.7	0

Iron (Fe) and Oxygen (O) which is the elements that compose the strontium hexaferrite. The elements percentage is in a virtuous covenant with the SrFe$_{12}$O$_{19}$ chemical composition, which verifies the contaminations nonexistence [31], except there exists a small amount of carbon element(C), as a contamination, which probably comes from the electrically conductive glue upon the holder of specimen or could be connected to the instrument sample carrier [1, 10].

And, the theoretical composition of elements percentages have been computed employing the this equation [1]:

$$x\% = z\frac{M_s}{M_T} \times 100 \qquad (4)$$

Where:
Ms: The element molar mass
M$_T$: The total molar mass
Z: The elements no.

And, the theoretical as well as the experimental weight percentages of the elements of strontium hexaferrite are tabulated in Table 5, for three different temperatures. The elements experimental weight percentage is in a good covenant with the theoretical values. Actually, the crystal structure manifested a uniform chemical composition.

Raman Measurements

Raman spectroscopy is a significant description process to analyze the M-type hexagonal ferrite structure. It's of a high significance to study the materials' lattice distortion [22]. And, in Raman spectroscopy, the incident phonons either lose quanta or gain quanta via interacting with the material vibrational modes. When it acquires

energy, it becomes blue-shifted, and when it misplaces, it's red-shifted. And, the shift quantity obtains the phonon energy in material [9]. The Raman spectra peaks are chiefly linked to the atomic bond vibration. Thus, a slight quantity of contaminations can be noticed. In this paper, Raman spectroscopy was has been utilized for studying the composition as well as the phases' uniformity in the system of SrFe$_{12}$O$_{19}$. Raman spectra of the neat SrM are shown in Fig. 8.

The strontium hexaferrite have been performed via comparing the noted outcomes with the chosen rules as well as the mode assignments debated via Kreisel et al. [32]. And, from the researches, it was documented that the (42) Raman-active modes (17E2g 11A1g + 14E1g + 17E2g) and (30 IR) active modes (13A2u + 17E1u) being anticipated for the system of hexaferrite. Also, the spectra of Raman have been obtained at the room temperature. The M-type strontium hexaferrite's hexagonal structure has been constructed of (5) layers: Three cubic blocks of S* and S with a spinel structure, and two hexagonal blocks of R* and R that contain the ion of Sr^{2+}. Such (5) layers make a single molecule, and (2) molecules make a single unit cell. And, the (24) ions of Fe^{3+} are dispersed above (5) various crystallographic locations, (3) octahedral locations (12k, 2a and 4f$_2$), (1) tetrahedral location (4f$_1$), and (1) trigonal-bipyramidal (2b) location, correspondingly. Spectra of the Raman of all samples in Fig. 8 reveals the sturdiest ions peak at almost (686 cm^{-1}), which being ascribed to the bipyramidal set motions (A1g) of the ions of Fe–O (site 2b) [33, 34]. A feeble peak was noted at a (725 cm^{-1}) frequency, which can be ascribed to the Fe–O ions movement (A$_{1g}$) at the (4f$_1$) tetrahedral locations. And, the 618 cm^{-1} as and 532 cm^{-1} bands are owing to the (A$_{1g}$) as well as the modes of the (E$_{1g}$) vibration of the bonds of Fe–O at the (4f$_2$)

Table 6. Most prominent Raman mode peaks of as-burnt and calcined at 1000 and 1100°C for SrFe$_{12}$O$_{19}$ nanopowder.

Temp.°C	Raman peaks (cm^{-1})						2b.A$_{1g}$
	E$_{1g}$	E$_{2g}$(1)	12k.A$_{1g}$ (2)	2a.A$_{1g}$ (1)	E$_{2g}$(2)	4f$_2$.A$_{1g}$	
as-burnt	282.36	338.70	407.86	471.15	532.35	616.12	686.79
1000	282.36	338.70	407.86	469.94	532.35	618.46	686.79
1100	282.36	338.70	409.09	471.15	532.35	618.46	687.94

octahedral location. Also, the 531 cm^{-1} and 469 cm^{-1} bands are owing to the modes of the (A$_{1g}$) vibration of the bonds of Fe–O at the (2a) octahedral location. Besides the overhead peaks, the samples' measured Raman spectra evinced that, other than the different bands widening, no fresh band was noted. And, this verifies that the samples being in a single-phase shape. The observed Raman spectra for most prominent peaks were indexed, and the relative condition of the noticed modes of vibration is shown in the Table 6. Such outcomes display slightly the shifts in some Raman modes of the (SrM) bands occurring toward the higher frequency values for Raman sites (12k.A$_{1g}$, 4f$_{2.}$A$_{1g}$, and 2b.A$_{1g}$). Such discrepancies are connected to

the length of chemical bond. The perceived values of peak frequency in spectra have been compared with those in the researches for the sole crystals, [33] nanoparticles [35], and polycrystalline [36]. It was been seen that they're in too virtuous covenant with those related with the sole crystals as well as nanoparticles. In Raman spectra, the peaks shifting toward the higher or lower wave no. is linked to the molecules' chemical bond length. And, the shorter length of bond reasons to move the higher wave no. or vice versa. When the length of the chemical bond of molecules varies owing to any interior or exterior influences, then it may result in a movement to the wave no. toward higher or lower frequencies.
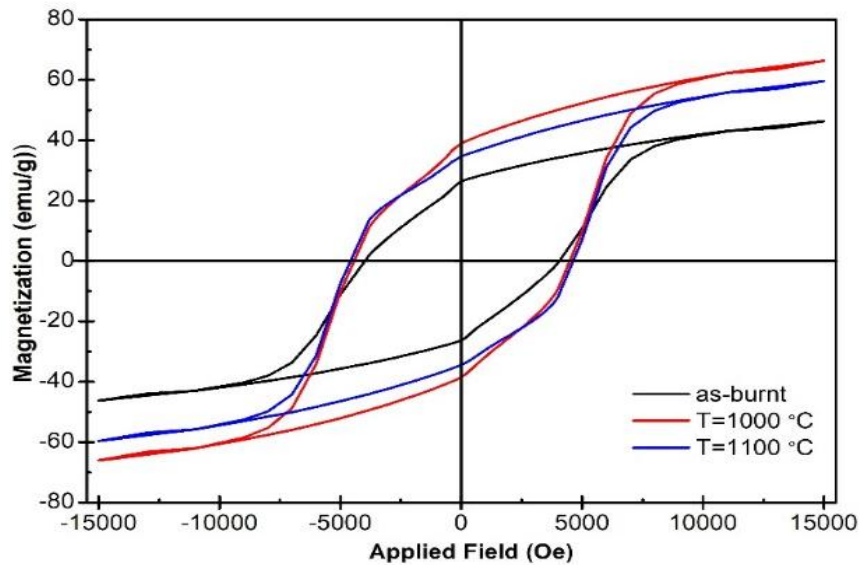

Fig. 9. The implemented-field dependency of the magnetization hysteresis loops of SrFe$_{12}$O$_{19}$ hexaferrite, at the room temperature.

Table 7. Magnetic parameters of SrFe$_{12}$O$_{19}$ for as burnt, and calcined at 1000°C and 1100°C.

Temp., °C	Ms (emu g^{-1})	Mr (emu g^{-1})	Hc(O$_e$)	Mr/Ms
As burnt	47.471	25.21	4610.0	0.531
1000	64.285	31.93	4464.0	0.496
1100	59.79	32.57	3995.0	0.544

Magnetic properties

Fig. 9 demonstrates the magnetic hysteresis loops of SrFe$_{12}$O$_{19}$ for as-burnt and calcined at temperatures (1000°C, 1100°C). The materials have been measured at a (±15 KOe) magnetic field at the room temperature. The whole investigated samples indicated a famous magnetic hysteresis with a ferromagnetic conduct noted. The of saturation magnetization (Ms) values for every sample was computed from the magnetic hysteresis loops utilizing the model of Stoner-Wolfforth (S-W), which being practicable for a sole domain [37, 38]. And, the magnetic factors, like coercivity (Hc), saturation magnetization (Ms), and remnant magnetization (Mr) have been obtained from the (M-H) loops and are listed in the Table 7. Moreover, the ratio of squareness (*S*) has been computed employing the subsequent equation [39, 40]:

$$S = \frac{M_r}{M_S} \qquad (5)$$

Form the results listed in Table 7 show the saturation magnetization (Ms) highest value is (66.2854 emu/g) performed at (15 KOe) for SrFe$_{12}$O$_{19}$, calcined at 1000°C, while the lowest value is (46.2680 emu/g) determined in the similar implemented field for the as-burnt temperature. It was confirmed that the calcination temperature has major influence on the saturation magnetization. The value of remnant magnetization (Mr) of the whole fabricated samples is ranged from (26.40 emu/g) to (34.57 emu/g), and such a behavior displays an increase of remnant magnetization with the increasing of calcined temperature of strontium hexaferrite. The squareness ratio (Mr/Ms) at calcined temperature of 1000°C for (SrM) was computed to be (0.496); the value under 0.5 is linked to the multi-magnetic domains. And, the obtained squareness value of (0.544) for a sample calcined at 1100°C, which being over a (0.5) theoretical value, signifying that the materials being a sole magnetic domain. In this paper, the noted value of Mr/Ms is too near to (0.5), proposing that the fabricated samples being in the sole magnetic domain [1, 41]. Fig. 9 manifests the Ms and Mr of as-burnt and calcined SrFe$_{12}$O$_{19}$ nanopowder at 1000°C and 1100°C.The obtained values of coercive field (Hc) were decreased in the range (4610.0-3995.0 O$_e$) with increasing calcined temperature of the synthesized MSr powder sample. In order to investigate the influence of calcined temperature on the behavior of saturation magnetization (Ms) and remnant magnetization
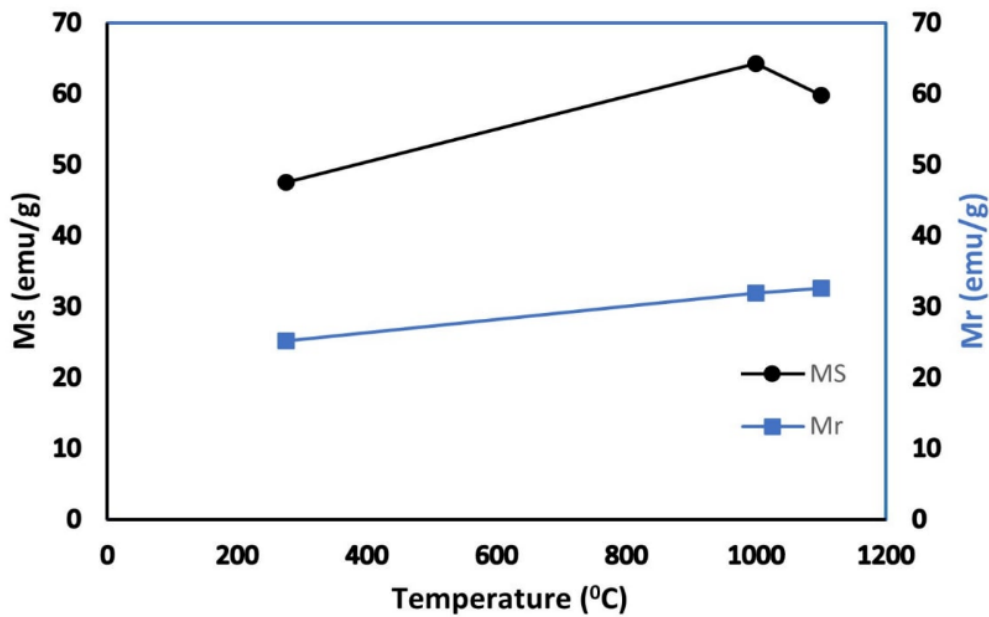

Fig. 10. Ms and Mr of as-burnt and calcined SrFe$_{12}$O$_{19}$ nanopowder at 1000°C and 1100°C.

(Mr), and Fig. 9 has been plotted for as-burnt and calcined temperatures at (1000 and 1100°C) of SrM nanopowders ferrite. Higher saturation and remnant magnetization value were found about (66.285 emu/g) and (38.90 emu/g), respectively for SrM calcined at 1000°C. The variation in magnetic characteristics can be ascribed to the crystalline size variation of the manufactured ferrite powders [13]. Furthermore, decreasing the (Fe/Sr) weight ratio as in Table 7 showed increasing the saturation magnetization (Ms) to (66.285 emu/g) and remnant magnetization to (38.9 emu/g) for calcined temperature 1000°C. And, this is owing to the decrease of the existence of Fe$_2$O$_3$ (0.7 wt.%) non-magnetic species. Also, the coercive force (Hc) of SrFe$_{12}$O$_{19}$ for as-burnt specimen has a higher value of (4610 Oe), and this lowered to (3995 Oe) with a decreased ratio of Fe$_2$O$_3$ up to zero at the calcined temperature of 1100°C. These results might be related to the residual Fe$_2$O$_3$ at lower calcined temperature having a higher intrinsic coercive force [42].

CONCLUSION

In this current investigation, the technique of sol-gel auto-combustion was obtained to be a simple, efficient and convenient route for preparing the M-type Sr hexaferrite nanopowder. And, the X-ray diffraction outcome manifested that the manufactured powder was a neat phase hexagonal crystal system with space group P63/mmc. The powders formed were investigated using Rietveld refinement (full-prof) program which evinces the decrease of lattice constants (a and c) with the calcined temperatures. FE-SEM, EDX, Raman spectroscopy and VSM technique were utilized for further investigation. And, the work elucidated that an increment in the calcination temperature resulted in the considerable rise in the crystallite size as well as the last product crystallinity. Also, the calculated crystallite size is increased up to (76.107 nm) for calcination temperature 1100°C. The obtained data confirmed that the prepared materials were SrM with different surface morphologies and particle sizes in the range (79.84 nm-295.5 nm) with increasing calcined temperature up to 1100°C. The magnetic properties including, Ms, Mr, SQR, and Hc were investigated. Although the saturation magnetization (Ms) does not reveal the clear calcination temperature dependence at all, while the magnetic remnant (Mr) and coercivity (Hc) depict the clear calcination temperature dependence.

CONFLICT OF INTEREST

The authors declare that there is no conflict of interests regarding the publication of this manuscript.

REFERENCES

1. Elansary M, Belaiche M, Ahmani Ferdi C, Iffer E, Bsoul I. New nanosized Gd-Ho-Sm doped M-type strontium hexaferrite for water treatment application: experimental and theoretical investigations. RSC advances. 2020;10(42):25239-25259.

2. Xie T, Xu L, Liu C. Synthesis and properties of composite magnetic material SrCoxFe$_{12-x}$O$_{19}$ (x=0–0.3). Powder Technol. 2012;232:87-92.

3. Ashiq MN, Shakoor S, Najam-ul-Haq M, Warsi MF, Ali I, Shakir I. Structural, electrical, dielectric and magnetic properties of Gd-Sn substituted Sr-hexaferrite synthesized by sol–gel combustion method. J Magn Magn Mater. 2015;374:173-178.

4. Kazin PE, Trusov LA, Zaitsev DD, Tretyakov YD, Jansen M. Formation of submicron-sized SrFe$_{12-x}$Al$_x$O$_{19}$ with very high coercivity. J Magn Magn Mater. 2008;320(6):1068-1072.

5. Morisako A, Naka T, Ito K, Takizawa A, Matsumoto M, Hong Y-K. Properties of Ba-ferrite/AlN double layered films for perpendicular magnetic recording media. J Magn Magn Mater. 2002;242-245:304-310.

6. Hernández P, de Francisco C, Muñoz JM, Iñiguez J, Torres L, Zazo M. Influence of sintering atmosphere on the magnetic after-effect in strontium ferrites. J Magn Magn Mater. 1996;157-158:123-124.

7. Iqbal MJ, Ashiq MN, Hernandez-Gomez P, Munoz JM. Synthesis, physical, magnetic and electrical properties of Al–Ga substituted co-precipitated nanocrystalline strontium hexaferrite. J Magn Magn Mater. 2008;320(6):881-886.

8. Yang Y, Liu X, Jin D. Influence of heat treatment temperatures on structural and magnetic properties of Sr$_{0.50}$Ca$_{0.20}$La$_{0.30}$Fe$_{11.15}$Co$_{0.25}$O$_{19}$ hexagonal ferrites. J Magn Magn Mater. 2014;364:11-17.

9. Khojaste khoo M, Kameli P. Structure and Magnetization of Strontium Hexaferrite (SrFe$_{12}$O$_{19}$) Films Prepared by Pulsed Laser Deposition. Frontiers in Materials. 2021;8.

10. Zi ZF, Sun YP, Zhu XB, Yang ZR, dai JM, Song WH. Structural and magnetic properties of SrFe$_{12}$O$_{19}$ hexaferrite synthesized by a modified chemical co-precipitation method. J Magn Magn Mater. 2008;320(21):2746-2751.

11. Pullar RC. Hexagonal ferrites: A review of the synthesis, properties and applications of hexaferrite ceramics. Prog Mater Sci. 2012;57(7):1191-1334.

12. Kools F, Morel A, Grössinger R, Le Breton JM, Tenaud P. LaCo-substituted ferrite magnets, a new class of high-grade ceramic magnets; intrinsic and microstructural aspects. J Magn Magn Mater. 2002;242-245:1270-1276.

13. Hessien MM, Rashad MM, El-Barawy K. Controlling the composition and magnetic properties of strontium hexaferrite synthesized by co-precipitation method. J Magn Magn Mater. 2008;320(3-4):336-343.

14. Al-Jumaili BEB, Talib ZA, Zakaria A, Ramizy A, Ahmed NM, Paiman SB, et al. Impact of ablation time on Cu oxide

nanoparticle green synthesis via pulsed laser ablation in liquid media. Appl Phys A. 2018;124(9).

15. Khodair ZT, Mohammad AM, Khadom AA. Investigations of structural and magnetic properties of Cu$_{1-x}$V$_x$O nanostructures prepared by sol-gel method. Chemical Data Collections. 2020;25:100315.

16. Akl AA, Hassanien AS. Microstructure and crystal imperfections of nanosized CdS Se1– thermally evaporated thin films. Superlattices Microstruct. 2015;85:67-81.

17. Augustin CO, Selvan RK, Nagaraj R, Berchmans LJ. Effect of La^{3+} substitution on the structural, electrical and electrochemical properties of strontium ferrite by citrate combustion method. Materials Chemistry and Physics. 2005;89(2-3):406-411.

18. Zhang Z, Jiang C, Fu P, Cai F, Ma N. Microstructure and texture of electrodeposited Ni–ZrC composite coatings investigated by Rietveld XRD line profile analysis. J Alloys Compd. 2015;626:118-123.

19. Sun K, Pu Z, Yang Y, Chen L, Yu Z, Wu C, et al. Rietveld refinement, microstructure and ferromagnetic resonance linewidth of iron-deficiency NiCuZn ferrites. J Alloys Compd. 2016;681:139-145.

20. Lala S, Satpati B, Pradhan SK. Sintering behavior and growth mechanism of β-TCP in nanocrystalline hydroxyapatite synthesized by mechanical alloying. Ceram Int. 2016;42(11):13176-13182.

21. Verma S, Rani S, Kumar S, Khan MAM. Rietveld refinement, micro-structural, optical and thermal parameters of zirconium titanate composites. Ceram Int. 2018;44(2):1653-1661.

22. Zhang W, Li P, Wang Y, Guo J, Li J, Shan S, et al. Structure, Spectra, Morphology, and Magnetic Properties of Nb^{5+} Ion-Substituted Sr Hexaferrites. Magnetochemistry. 2022;8(5):51.

23. Chen D-H, Chen Y-Y. Synthesis of strontium ferrite nanoparticles by coprecipitation in the presence of polyacrylic acid. Mater Res Bull. 2002;37(4):801-810.

24. Kimura K, Ohgaki M, Tanaka K, Morikawa H, Marumo F. Study of the bipyramidal site in magnetoplumbite-like compounds, SrM$_{12}$O$_{19}$ (M = Al, Fe, Ga). J Solid State Chem. 1990;87(1):186-194.

25. Wagner TR. Preparation and Crystal Structure Analysis of Magnetoplumbite-Type BaGa$_{12}$O$_{19}$. J Solid State Chem. 1998;136(1):120-124.

26. Ramkumar T, Selvakumar M, Vasanthsankar R, Sathishkumar AS, Narayanasamy P, Girija G. Rietveld refinement of powder X-ray diffraction, microstructural and mechanical studies of magnesium matrix composites processed by high energy ball milling. Journal of Magnesium and Alloys. 2018;6(4):390-398.

27. Collomb A, Lambert-Andron B, Boucherle JX, Samaras D. Crystal Structure and Cobalt Location in the W-Type Hexagonal Ferrite [Ba]Co2-W. physica status solidi (a). 1986;96(2):385-395.

28. Park J, Hong Y-K, Kim S-G, Kim S, Liyanage LSI, Lee J, et al. Maximum energy product at elevated temperatures for hexagonal strontium ferrite (SrFe$_{12}$O$_{19}$) magnet. J Magn Magn Mater. 2014;355:1-6.

29. Almessiere MA, Slimani Y, El Sayed HS, Baykal A. Structural and magnetic properties of Ce-Y substituted strontium nanohexaferrites. Ceram Int. 2018;44(11):12511-12519.

30. WITHDRAWN: Zinc Substituted Nickel-cobalt Nano-ferrites via Citrate-gel Auto-combustion Method for High-frequency Applications: Studies on Crystal Structure and Dielectric Properties. Research Square Platform LLC; 2021.

31. Khan HM, Islam MU, Xu Y, Iqbal MA, Ali I, Ishaque M, et al. Structural, magnetic, and microwave properties of NdZn-substituted Ca$_{0.5}$Ba$_{0.5}$Fe$_{12}$O$_{19}$ hexaferrites. J Sol-Gel Sci Technol. 2015;75(2):305-312.

32. Kreisel J, Pignard S, Vincent H, Sénateur JP, Lucazeau G. Raman study of BaFe$_{12}$O$_{19}$ thin films. Appl Phys Lett. 1998;73(9):1194-1196.

33. Kreisel J, Lucazeau G, Vincent H. Raman Spectra and Vibrational Analysis of BaFe$_{12}$O$_{19}$ Hexagonal Ferrite. J Solid State Chem. 1998;137(1):127-137.

34. Morel A, Le Breton JM, Kreisel J, Wiesinger G, Kools F, Tenaud P. Sublattice occupation in Sr$_{1-x}$La$_x$Fe$_{12-x}$Co$_x$O$_{19}$ hexagonal ferrite analyzed by Mössbauer spectrometry and Raman spectroscopy. J Magn Magn Mater. 2002;242-245:1405-1407.

35. Anbarasu V, Md Gazzali PM, Karthik T, Manigandan A, Sivakumar K. Effect of divalent cation substitution in the magnetoplumbite structured BaFe$_{12}$O$_{19}$ system. Journal of Materials Science: Materials in Electronics. 2012;24(3):916-926.

36. Chen MS, Shen ZX, Liu XY, Wang J. Raman and magnetization studies of barium ferrite powder prepared by water-in-oil microemulsion. J Mater Res. 2000;15(2):483-487.

37. Stoner EC, Wohlfarth EP. A mechanism of magnetic hysteresis in heterogeneous alloys. IEEE Trans Magn. 1991;27(4):3475-3518.

38. Almessiere MA, Slimani Y, Baykal A. Structural and magnetic properties of Ce-doped strontium hexaferrite. Ceram Int. 2018;44(8):9000-9008.

39. Abuzir AR, Salman SA, Mazher J. Magnetron Sputtered Perpendicular Barium Hexaferrite Thin Films Produced by the Multilayered Method. Journal of Superconductivity and Novel Magnetism. 2020;33(12):3819-3825.

40. Digest Journal of Nanomaterials and Biostructures.

41. Mouhib Y, Belaiche M, Briche S. Elaboration, Characterization, and Magnetic Properties of Ni$_{0.5}$Zn$_{0.5}$Fe$_2$O$_4$ Nanoparticles of High Purity Using Molten Salts Technique. physica status solidi (a). 2018;215(23).

42. Fu Y-P, Lin C-H. Fe/Sr ratio effect on magnetic properties of strontium ferrite powders synthesized by microwave-induced combustion process. J Alloys Compd. 2005;386(1-2):222-227.